ELSEVIER

Engineering Analysis with Boundary Elements 29 (2005) 241–256

ENGINEERING ANALYSIS *with* BOUNDARY ELEMENTS

www.elsevier.com/locate/enganabound

Analytical evaluation and application of the singularities in boundary element method

John Wang*, Ting-Kuei Tsay

Department of Civil Engineering, National Taiwan University, Taipei, Taiwan, ROC

Received 8 January 2004; revised 4 May 2004; accepted 17 December 2004
Available online 19 March 2005

Abstract

In this paper, two alternative approaches to the boundary element method (BEM) are investigated; namely, the contour approach method and the direct approach method. A detailed comparison of these methods is made by evaluating the accuracy of singular boundary integrals. A complete and comprehensive exposition of the derivation leads to the correct implementation. This is in contrast to conventional numerical integration methods, which suffer from the numerical boundary layer. Singularities which are mathematical artifacts are shown to vanish when the contour approach and the direct approach methods are applied. Singularities which arise from the physics are dealt with by way of a complex mapping method in the BEM. The results of seven benchmark problems which are supportive of these conclusions are presented at the end of this article.

Keywords: Boundary element method; Singularities; Cut-off wall; Numerical boundary layer

1. Introduction

So-called mathematical singularities arise as a result of the Laplace operator, introduced into the governing equation by the application of the method of weighted residuals. A simple, 2D Laplace equation is adequate for the investigation of these mathematical singularities.

The integral equation for 2D potential problems can be represented as follows

$$c(P)\Phi(P) = \int_{\Gamma} \left(\frac{\Phi(Q)}{r(P,Q)} \frac{\partial r(P,Q)}{\partial n} - \ln r(P,Q) \frac{\partial \Phi(Q)}{\partial n} \right) \mathrm{d}s \tag{1}$$

where Γ is the boundary, n is the outward normal to this boundary, Φ is the potential and r is the distance between the source and field points, P and Q, respectively. The free-term coefficient, $c(P)$, is 2π when P lies inside the boundary and internal angle, α, when P lies on the boundary. It was originally thought that the mathematical singularity arises from the fact that the term $1/r(P,Q)$ in Eq. (1) approaches infinite if P is placed on the boundary. The unbounded term causes the solution to diverge and some special techniques are necessary to circumvent this problem. The Cauchy principal value (CPV) integral is one such method and involves deforming the integration path around the singular point, using a segment of a circle (in 2D) or sphere (in 3D), then shrinking the contour to the singular point [1]. (Of course, the contour shape is not necessarily restricted to a circular arc or spherical surface. A symmetric neighborhood can, however, simplify manipulations, although contour shape itself has no bearing whatsoever on the final value of the limit [2,3].)

Conventional wisdom has it that a numerical boundary layer is brought into existence when the source point is placed very close to the boundary [4–6]. For singularities, a popular method to integration is to use Gaussian quadrature rules integration [7]. Besides, Mapping techniques by Guiggiani [3], Johnston [8], and Nagarajan [9] are used for regularization, thereby avoiding the mathematical singularity. The bicubic transformation method of Charles [10] and the non-linear transformations by Krishna [11] are alternative means to treat the singularity problems associated with the BEM.

In this paper, singularity problems in BEM are divided in two categories: mathematical singularities and physical

* Corresponding author.
E-mail address: d89521008@ntu.edu.tw (J. Wang).

0955-7997/$ - see front matter © 2005 Elsevier Ltd. All rights reserved.
doi:10.1016/j.enganabound.2004.12.008

singularities. The former arises as a result of the coincidence of the source point with the field point while the latter is associated with the degeneration of the boundary (i.e. geometrical singularities) or a discontinuity in boundary conditions. It is the crux of this article that the former is a non-existent mathematical artifact and the latter type may be overcome by means of an involved mapping technique.

It is important to note that the mathematical singularities can be shown to vanish when obtaining solutions of physically non-singular problems [12,13]. Simple and straightforward proofs are presented for the contour and the direct approach methods to BEM. A thorough exposition of numerical boundary layers attempts to dispel any misperceptions which have arisen in the past.

Benchmark problems of a corner, a cut-off wall, and crack problems are revisited for the case of physical singularities. Methods such as the multiple node method [14], the iterative solution method of BEM [15], the floating node method by Gupta [16], the adaptive mesh refinement method [17] and the hyper-singular integrals or dual boundary integral method have been studied previously for corner problems [18–20]. Furthermore, the singular element method [4] and the multi-domain method [21] are adopted to conquer these singular problems. In fact, after the development of the dual BEM by Hong and Chen [22] in 1988, the dual boundary integral method [20,23,24] seems to be the most popular means of dealing with problems such as cut-off wall or crack problems. The displacement discontinuity method [25], the crack Green's function method [26], and multi-domain or dual boundary integral method are also applied to crack problems [27,28].

Mapping techniques have also been extensively applied in dealing with these singularity related problems. The so-called mathematical singularity is a mathematical artefact and the mapping methods developed are a means to resolve physical singularities alone. Numerical mapping techniques such as the Cauchy integral element method by Detournay [29,30] and conformal mapping by Papamichael [31–33] are efficient and accurate in dealing with physical singularities in addition to the transformation methods mentioned above.

The objective of this paper is to deal with the singularity problems in BEM in two respects. To identify the artificial nature of mathematical singularities in BEM [13] and to demonstrate a method of overcoming true, physically existent singularities. It is to be noted that the contour approach method and the direct approach method are not the methods beyond the conventional boundary element, except the correct evaluation of the integral to discrete elements analytically in BEM. In the former method, the procedures are all the same as the conventional BEM except the correction of an angle term within the integral. This correction, however, will not affect the results. It presents a right procedure for treating the integral. The importance of the conception is its application to the direct approach method. After the evaluation of the boundary potentials and their derivatives with contour approach method, the direct approach method re-evaluate the potentials on the boundary by moving the interior source points toward the boundary as near as possible but not on the boundary so as to find that the potential converges to that by the contour approach method. In this way, the so-called numerical boundary layer can be proved to be non-existent [4–6].

2. Mathematical singularities in BEM

2.1. Discretization of boundary integral equation

For discretization of the boundary integral equation to boundary elements, linear elements are introduced to represent the geometry and the boundary fields in terms of nodal values and their derivatives, that is

$$\Phi = [(\Phi_{j+1} - \Phi_j)\xi + (\xi_{j+1}\Phi_j - \xi_j\Phi_{j+1})]/(\xi_{j+1} - \xi_j)$$

$$\frac{\partial \Phi}{\partial n} = \left\{ \left[\left(\frac{\partial \Phi}{\partial n}\right)_{j+1} - \left(\frac{\partial \Phi}{\partial n}\right)_{j} \right] \xi + \left[\xi_{j+1}\left(\frac{\partial \Phi}{\partial n}\right)_{j} - \xi_j \left(\frac{\partial \Phi}{\partial n}\right)_{j+1} \right] \right\} / (\xi_{j+1} - \xi_j)$$

$$\xi_j \le \xi \le \xi_{j+1} \tag{2}$$

where an element-wise local coordinates ξ-η is defined in Fig. 1. The subscripts j and $j+1$ represent the starting and ending nodes of the element, respectively. The analytical form of the integral equation, Eq. (1), can then be shown as [4]

$$c(P)\Phi(P) = \sum_{e=1}^{n} I^e \tag{3}$$

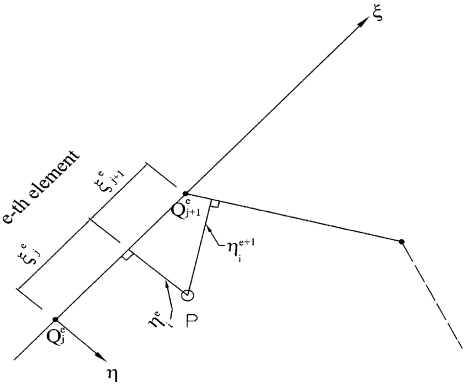

Fig. 1. Definition of element-wise ξ–η local coordinate.

where

$$I^e = \int_{\xi_j}^{\xi_{j+1}} \left(\frac{\Phi}{r} \frac{\partial r}{\partial n} - \ln r \frac{\partial \Phi}{\partial n} \right) \mathrm{d}\xi = [K_1^e] \begin{bmatrix} \Phi_j^e \\ \Phi_{j+1}^e \end{bmatrix} - [K_2^e] \begin{bmatrix} \left(\frac{\partial \Phi}{\partial n} \right)_j^e \\ \left(\frac{\partial \Phi}{\partial n} \right)_{j+1}^e \end{bmatrix} \tag{4}$$

$$K_1^e = [-I_{11}^e + \xi_{j+1}^e I_{12}^e \quad I_{11}^e - \xi_j^e I_{12}^e]$$
$$K_2^e = [-I_{21}^e + \xi_{j+1}^e I_{22}^e \quad I_{21}^e - \xi_j^e I_{22}^e] \tag{5}$$

and

$$I_{11}^e = \frac{1}{(\xi_{j+1}^e - \xi_j^e)} \int_{\xi_j}^{\xi_{j+1}} \frac{1}{r} \frac{\partial r_i}{\partial n} \xi \, \mathrm{d}\xi = \frac{1}{2} \eta_i^e \ln \left[\frac{(\eta_i^e)^2 + (\xi_{j+1}^e)^2}{(\eta_i^e)^2 + (\xi_j^e)^2} \right] / (\xi_{j+1}^e - \xi_j^e) \tag{6}$$

$$I_{12}^e = \frac{1}{(\xi_{j+1}^e - \xi_j^e)} \int_{\xi_j}^{\xi_{j+1}} \frac{1}{r} \frac{\partial r_i}{\partial n} \mathrm{d}\xi = \left[\tan^{-1} \left(\frac{\xi_{j+1}^e}{\eta_i^e} \right) - \tan^{-1} \left(\frac{\xi_j^e}{\eta_i^e} \right) \right] / (\xi_{j+1}^e - \xi_j^e) \tag{7}$$

$$I_{21}^e = \frac{1}{(\xi_{j+1}^e - \xi_j^e)} \int_{\xi_j}^{\xi_{j+1}} \ln(r_i) \xi \, \mathrm{d}\xi = \frac{1}{4} \{ [(\eta_i^e)^2 + (\xi_{j+1}^e)^2][\ln((\eta_i^e)^2 + (\xi_{j+1}^e)^2) - 1] - [(\eta_i^e)^2 + (\xi_j^e)^2][\ln((\eta_i^e)^2 + (\xi_j^e)^2) - 1] \} / (\xi_{j+1}^e - \xi_j^e) \tag{8}$$

$$I_{22}^e = \frac{1}{(\xi_{j+1}^e - \xi_j^e)} \int_{\xi_j}^{\xi_{j+1}} \ln(r_i) \mathrm{d}\xi = \frac{1}{2} \left\{ \xi_{j+1}^e \ln[(\eta_i^e)^2 + (\xi_{j+1}^e)^2] - \xi_j^e \ln[(\eta_i^e)^2 + (\xi_j^e)^2] - 2(\xi_{j+1}^e - \xi_j^e) + 2\eta_i^e \left[\tan^{-1} \left(\frac{\xi_{j+1}^e}{\eta_i^e} \right) - \tan^{-1} \left(\frac{\xi_j^e}{\eta_i^e} \right) \right] \right\} / (\xi_{j+1}^e - \xi_j^e) \tag{9}$$

The superscript e represents the eth element on the boundary and the subscript i represents the ith source point. To obtain the potential on the boundary, two methods are adopted in this paper. The first one, contour approach method, places the source point on the boundary and apply a detoured integration path represented by a shrinking arc. The second one, direct approach method, evaluates the potential of the boundary point Q by moving the source point P towards Q along an arbitrary straight path.

For brevity, only the concerned elements I^m and I^{m+1} are discussed as the source point P is put on or moved towards the mth node where the mathematical singularity problems may occur as it seems. On the other hand, the case for the source point on the boundary is of the same approach as on the node and will not be stated repeatedly in this paper. Eq. (3) can then be rewritten as

$$c(P)\Phi(P) = \left(\sum_{e=1}^{m-1} I^e \right) + I^m + I^{m+1} + \left(\sum_{e=m+2}^{n} I^e \right) \tag{10}$$

where the first and the last terms on the right hand side of Eq. (10) are irrelevant to the matter concerning on singularity.

2.2. Contour approach method

When the source point is put directly on the Q_m node as shown in Fig. 2, a shrinking arc contour composed of $Q_m^- Q_m^+$ is used to exclude the source point, the integrations of Eqs. (6)–(9) can be evaluated with the following process:

(1) For either mth or $(m+1)$th element, $\eta_i = 0$ in this case.
(2) θ_j^m and θ_{j+1}^m, as defined in Fig. 2, approach $-\pi/2$ in the limiting state the shrinking arc converging to the source point. Similarly, θ_j^{m+1} and θ_{j+1}^{m+1} are $\pi/2$ in that situation.
(3) ξ_j^m, the distance between the source point and the starting nodal point of mth element, as defined in Fig. 1, equals to the length of mth element, $-l^m$. In the same way, $\xi_{j+1}^m = 0$, $\xi_j^{m+1} = 0$ and $\xi_{j+1}^{m+1} = l^{m+1}$.
(4) According to the previous results, the integral value for I_{11}, I_{12}, I_{21} and I_{22} are

$$I_{11}^m = \frac{1}{2} \eta_i^m \ln \left[\frac{(\eta_i^m)^2 + (\xi_{j+1}^m)^2}{(\eta_i^m)^2 + (\xi_j^m)^2} \right] / (\xi_{j+1}^m - \xi_j^m) = 0$$

$$I_{12}^m = \left[\tan^{-1} \left(\frac{\xi_{j+1}^m}{\eta_i^m} \right) - \tan^{-1} \left(\frac{\xi_j^m}{\eta_i^m} \right) \right] / (\xi_{j+1}^m - \xi_j^m) = (\theta_{j+1}^m - \theta_j^m) / l^m = 0$$

$$I_{21}^m = \frac{1}{4} \{ [(\eta_i^m)^2 + (\xi_{j+1}^m)^2][\ln((\eta_i^m)^2 + (\xi_{j+1}^m)^2) - 1] - [(\eta_i^m)^2 + (\xi_j^m)^2][\ln((\eta_i^m)^2 + (\xi_j^m)^2) - 1] \} / (\xi_{j+1}^m - \xi_j^m) = \frac{1}{4} [-(l^m)^2 (2 \ln l^m - 1)] / l^m$$

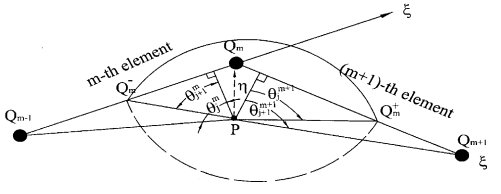

Fig. 2. Illustrations of the contour method.

$$I_{22}^m = \frac{1}{2}\Bigg\{\xi_{j+1}^m \ln[(\eta_i^m)^2 + (\xi_{j+1}^m)^2] - \xi_j^m \ln[(\eta_i^m)^2 + (\xi_j^m)^2] - 2(\xi_{j+1}^m - \xi_j^m) + 2\eta_i^m\left[\tan^{-1}\left(\frac{\xi_{j+1}^m}{\eta_i^m}\right) - \tan^{-1}\left(\frac{\xi_j^m}{\eta_i^m}\right)\right]\Bigg\}/(\xi_{j+1}^m - \xi_j^m) = -(\ln l^m + 1)$$

$$I_{11}^{m+1} = \frac{1}{2}\eta_i^{m+1}\ln\left[\frac{(\eta_i^{m+1})^2 + (\xi_{j+1}^{m+1})^2}{(\eta_i^{m+1})^2 + (\xi_j^{m+1})^2}\right]/(\xi_{j+1}^m - \xi_j^m) = 0$$

$$I_{12}^{m+1} = \left[\tan^{-1}\left(\frac{\xi_{j+1}^{m+1}}{\eta_i^{m+1}}\right) - \tan^{-1}\left(\frac{\xi_j^{m+1}}{\eta_i^{m+1}}\right)\right]\Big/ (\xi_{j+1}^{m+1} - \xi_j^{m+1}) = (\theta_{j+1}^{m+1} - \theta_j^{m+1})/l^{m+1} = 0$$

$$I_{21}^{m+1} = \frac{1}{4}\{[(\eta_i^{m+1})^2 + (\xi_{j+1}^{m+1})^2][\ln((\eta_i^{m+1})^2 + (\xi_{j+1}^{m+1})^2) - 1] - [(\eta_i^{m+1})^2 + (\xi_j^{m+1})^2][\ln((\eta_i^{m+1})^2 + (\xi_j^{m+1})^2) - 1]\}/(\xi_{j+1}^{m+1} - \xi_j^{m+1}) = \frac{1}{4}[(l^{m+1})^2(2\ln l^{m+1} - 1)]/l^{m+1}$$

$$I_{22}^{m+1} = \frac{1}{2}\Bigg\{\xi_{j+1}^{m+1}\ln[(\eta_i^{m+1})^2 + (\xi_{j+1}^{m+1})^2] - \xi_j^{m+1}\ln[(\eta_i^{m+1})^2 + (\xi_j^{m+1})^2] - 2(\xi_{j+1}^{m+1} - \xi_j^{m+1}) + 2\eta_i^{m+1}\left[\tan^{-1}\left(\frac{\xi_{j+1}^{m+1}}{\eta_i^{m+1}}\right) - \tan^{-1}\left(\frac{\xi_j^{m+1}}{\eta_i^{m+1}}\right)\right]\Bigg\}\Big/ (\xi_{j+1}^{m+1} - \xi_j^{m+1}) = (\ln l^{m+1} + 1) \quad (11)$$

where l^m and l^{m+1} are lengths of mth and $(m+1)$th elements.

When I_{12}^m is considered, it should be noted that the angles θ_j^m and θ_{j+1}^m are not really zeroes as it was mistakenly taken when the source point P is put on the node (Fig. 2). It is indicated that the angle θ_{j+1}^m is related to point Q_m^-, not Q_m, which has been excluded from the integral path. The angles of θ_j^m and θ_{j+1}^m remain $-\pi/2$ for both ends on the mth element and θ_j^{m+1} and θ_{j+1}^{m+1} are $\pi/2$ for the ends of $(m+1)$th element in the process of the contour shrinking to the nodal point (Fig. 2). Thus, the integral of I_{12}^m becomes zero, not $-\pi/2l^m$. Similarly, I_{12}^{m+1} is zero instead of $-\pi/2l^{m+1}$. This is beyond the accepted conception that the r^{-1} and r^{-2} integrations cannot be integrated for one-side limit and the combined limits exist only when constant ratio's limit of the two-side is applied [34]. Present results show that integration limits exist without any constraints.

It is of interest to know the errors contributed by the wrong estimations of I_{12}^m and I_{12}^{m+1} to the whole boundary integral, $\sum_{e=1}^n I^e$, in Eq. (3). Let $E^m = -\pi/2l^m$ and $E^{m+1} = -\pi/2l^{m+1}$, and referring to the assumption of linear distribution of Φ along the boundary, the errors, E, derived from Eqs. (2)–(5), can be expressed as

$$\begin{aligned} E &= \xi_{j+1}^m E^m \Phi_j^m - \xi_j^m E^m \Phi_{j+1}^m + \xi_{j+1}^{m+1} E^{m+1}\Phi_j^{m+1} - \xi_j^{m+1}E^{m+1}\Phi_{j+1}^{m+1} \\ &= E^m[(\xi_{j+1}^m - \xi_p)\Phi_j^m + (\xi_p - \xi_j^m)\Phi_{j+1}^m - (\Phi_{j+1}^m - \Phi_j^m)\xi_p] \\ &\quad + E^{m+1}[(\xi_{j+1}^{m+1} - \xi_p)\Phi_j^{m+1} + (\xi_p - \xi_j^{m+1})\Phi_{j+1}^{m+1} - (\Phi_{j+1}^{m+1} - \Phi_j^{m+1})\xi_p] = (E^m \cdot l^m + E^{m+1}\cdot l^{m+1})\Phi(p) \\ &= -\pi\Phi(p) \end{aligned} \quad (12)$$

where $\xi_P = 0$.

The result reveals that a value of $\pi\Phi(p)$ is underestimated due to the incorrect estimation of angle terms. If one has done the boundary element integration correctly, consistent results must be obtained when the field point is either on the boundary or as an interior point approaching the boundary. In this way the errors, leading to the traditional inference that there is a numerical boundary layer or a jump term, are corrected. In Section 2.3, the inference will be discussed more formally and a new insight is proposed.

2.3. Direct approach method

When the source point is treated as an interior point and moved infinitesimally towards the node Q_{m+1} along a straight path, $\overline{PQ_{m+1}}$ with an arbitrary angle γ relative to η direction (Fig. 3(a)–(c)), the limits of the integrations in Eqs. (6)–(9) are calculated according to the following algorithms:

(1) For either mth or $(m+1)$th element, $\eta_i = 0$ in all cases.
(2) For the case of sharp interior angle α as shown in Fig. 3(a), θ_j^m and θ_{j+1}^m approach γ and $-\pi/2$, respectively, when the interior source point P moves toward the nodal point. Meanwhile, θ_j^{m+1} and θ_{j+1}^{m+1} approach $\pi-\gamma-\alpha$ and $\pi/2$, respectively, in the limiting process.
(3) ξ_j^m, the same as that in the contour approach method, equals to the length of mth element, $-l^m$. Likewise, $\xi_{j+1}^m = 0$, $\xi_j^{m+1} = 0$ and $\xi_{j+1}^{m+1} = l^{m+1}$.
(4) According to the previous results, the integral values for I_{11}, I_{12}, I_{21} and I_{22} are

$$I_{11}^m = \frac{1}{2}\eta_i^m \ln\left[\frac{(\eta_i^m)^2 + (\xi_{j+1}^m)^2}{(\eta_i^m)^2 + (\xi_j^m)^2}\right]/(\xi_{j+1}^m - \xi_j^m) = 0$$

$$I_{12}^m = \left[\tan^{-1}\left(\frac{\xi_{j+1}^m}{\eta_i^m}\right) - \tan^{-1}\left(\frac{\xi_j^m}{\eta_i^m}\right)\right]\Big/(\xi_{j+1}^m - \xi_j^m) = (-\gamma + \pi/2)/l^m$$

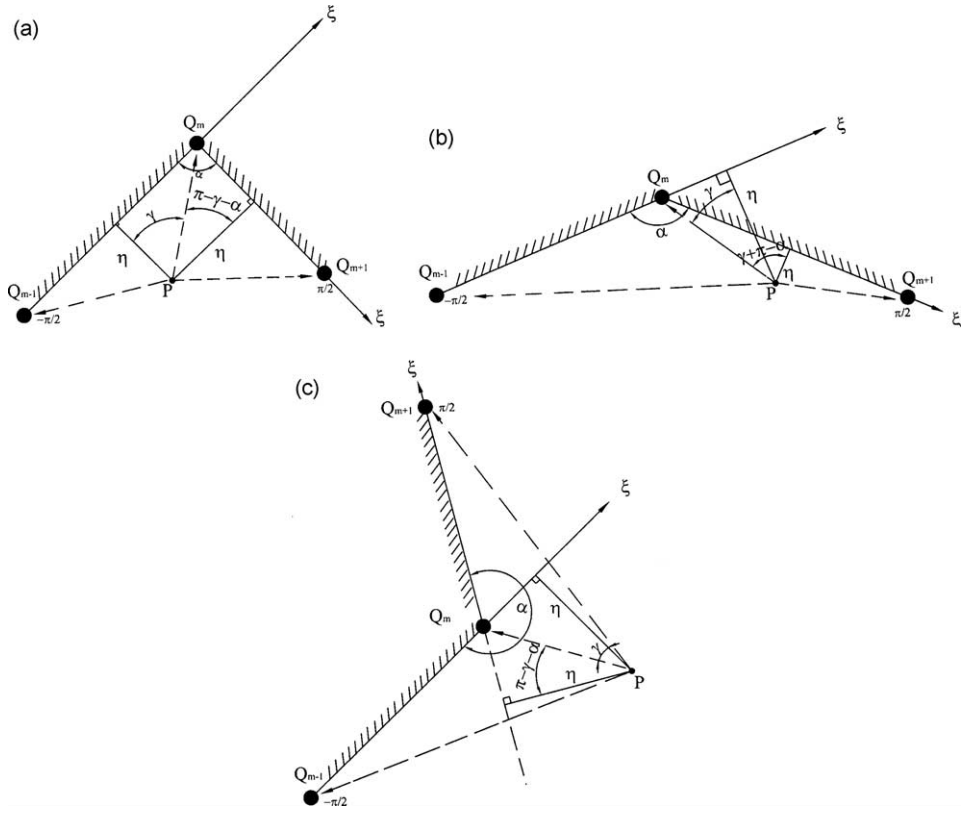

Fig. 3. (a) When $\alpha<90°$. (b) When $90°<\alpha<180°$. (c) When $180°<\alpha<360°$.

$$I_{21}^{m}=\frac{1}{4}\{[(\eta_i^m)^2+(\xi_{j+1}^m)^2][\ln((\eta_i^m)^2+(\xi_{j+1}^m)^2)-1]-[(\eta_i^m)^2+(\xi_j^m)^2][\ln((\eta_i^m)^2+(\xi_j^m)^2)-1]\}\Big/(\xi_{j+1}^m-\xi_j^m)=\frac{1}{4}[-(l^m)^2(2\ln l^m-1)]/l^m$$

$$I_{22}^{m}=\frac{1}{2}\left\{\xi_{j+1}^m\ln[(\eta_i^m)^2+(\xi_{j+1}^m)^2]-\xi_j^m\ln[(\eta_i^m)^2+(\xi_j^m)^2]-2(\xi_{j+1}^m-\xi_j^m)+2\eta_i^m\left[\tan^{-1}\left(\frac{\xi_{j+1}^m}{\eta_i^m}\right)-\tan^{-1}\left(\frac{\xi_j^m}{\eta_i^m}\right)\right]\right\}/(\xi_{j+1}^m-\xi_j^m)=-(\ln l^m+1)$$

$$I_{11}^{m+1}=\frac{1}{2}\eta_i^{m+1}\ln\left[\frac{(\eta_i^{m+1})^2+(\xi_{j+1}^{m+1})^2}{(\eta_i^{m+1})^2+(\xi_j^{m+1})^2}\right]/(\xi_{j+1}^m-\xi_j^m)=0$$

$$I_{12}^{m+1}=\left[\tan^{-1}\left(\frac{\xi_{j+1}^{m+1}}{\eta_i^{m+1}}\right)-\tan^{-1}\left(\frac{\xi_j^{m+1}}{\eta_i^{m+1}}\right)\right]\Big/(\xi_{j+1}^{m+1}-\xi_j^{m+1})=(\theta_{j+1}^{m+1}-\theta_j^{m+1})/l^{m+1}=[\pi/2+(\gamma+\pi-\alpha)]$$

$$I_{21}^{m+1}=\frac{1}{4}\{[(\eta_i^{m+1})^2+(\xi_{j+1}^{m+1})^2][\ln((\eta_i^{m+1})^2+(\xi_{j+1}^{m+1})^2)-1]-[(\eta_i^{m+1})^2+(\xi_j^{m+1})^2][\ln((\eta_i^{m+1})^2+(\xi_j^{m+1})^2)-1]\}/(\xi_{j+1}^{m+1}-\xi_j^{m+1})=\frac{1}{4}[(l^{m+1})^2(2\ln l^{m+1}-1)]/l^{m+1}$$

$$I_{22}^{m+1}=\frac{1}{2}\left\{\xi_{j+1}^{m+1}\ln[(\eta_i^{m+1})^2+(\xi_{j+1}^{m+1})^2]-\xi_j^{m+1}\ln[(\eta_i^{m+1})^2+(\xi_j^{m+1})^2]-2(\xi_{j+1}^{m+1}-\xi_j^{m+1})+2\eta_i^{m+1}\left[\tan^{-1}\left(\frac{\xi_{j+1}^{m+1}}{\eta_i^{m+1}}\right)-\tan^{-1}\left(\frac{\xi_j^{m+1}}{\eta_i^{m+1}}\right)\right]\right\}\Big/(\xi_{j+1}^{m+1}-\xi_j^{m+1})=(\ln l^{m+1}+1) \quad (13)$$

It is noted that the previous results are the same for the case of interior angel greater than 90° and less than 180°, and the case of interior angel greater than 180°, as shown in Fig. 3(b) and (c).

By comparing the difference between the contour approach method and the direct approach method, it can be found that the values of I_{12}^{m} and I_{12}^{m+1} in these two methods are not the same. In the direct approach method, it can be

seen from Fig. 3(a) that θ_{j+1}^m in I_{12}^m and θ_j^{m+1} in I_{12}^{m+1} remains the angles of $-\gamma$ and $-(\pi-\gamma-\alpha)$ as the source point approaches nodal point Q_m. The same as contour approach method, θ_j^m in I_{12}^m and θ_{j+1}^{m+1} in I_{12}^{m+1} approach $-\pi/2$ and $\pi/2$.

Thus, in evaluating the potential on the mth node, the difference of the two methods on the right hand side of Eq. (10) is

$$\begin{aligned}
&(I'^m + I'^m{+}1) - (I^m + I^{m+1}) \\
&\quad = \xi_{j+1}^m D^m \Phi_j^m - \xi_j^m D^m \Phi_{j+1}^m + \xi_{j+1}^{m+1} D^{m+1} \Phi_j^{m+1} \\
&\qquad - \xi_j^{m+1} D^{m+1} \Phi_{j+1}^{m+1} \\
&\quad = D^m[(\xi_{j+1}^m - \xi_p)\Phi_j^m + (\xi_p - \xi_j^m)\Phi_{j+1}^m \\
&\qquad - (\Phi_{j+1}^m - \Phi_j^m)\xi_p] + D^{m+1}[(\xi_{j+1}^{m+1} - \xi_p)\Phi_j^{m+1} \\
&\qquad + (\xi_p - \xi_j^{m+1})\Phi_{j+1}^{m+1} - (\Phi_{j+1}^{m+1} - \Phi_j^{m+1})\xi_p] \\
&\quad = (D^m \cdot l^m + D^{m+1} \cdot l^{m+1})\Phi(p) = (2\pi - \alpha)\Phi(p) \qquad (14)
\end{aligned}$$

where $\xi_p = 0$, $D^m = [-\gamma + (\pi/2)]/l^m$, and $D^{m+1} = [\pi/2 + (\gamma + \pi - \alpha)]/l^{m+1}$.

The same result can also be reached when different types of interior angles in Fig. 3(b) and (c) are considered.

For different concepts of contour and direct approach methods, the discretized boundary element integral equation, Eq. (10), can be written, respectively, as:

$$\alpha\Phi(P) = \left(\sum_{e=1}^{m-1} I^e\right) + I^m + I^{m+1} + \left(\sum_{e=m+2}^{n} I^e\right) \qquad (15)$$

$$2\pi\Phi(P) = \left(\sum_{e=1}^{m-1} I^e\right) + I'^m + I'^{m+1} + \left(\sum_{e=m+2}^{n} I^e\right) \qquad (16)$$

It is obvious that Eqs. (15) and (16) are identical when Eq. (14) is substituted into Eq. (16). This result indicates that Eq. (16) can be applied anywhere on the domain, including the boundary, with correct evaluations of the integration on the right hand side of Eq. (1). It also reveals that the source point can be located anywhere—from the interior to the boundary of the domain, without any hindering from mathematical singularity. The continuity of the numerical results in the boundary approaching process is then expected. Present formulations step-by-step show that both the contour approach method and the direct approach method perform correctly. It does not require special complicated mathematical manipulation. Meanwhile, it plays an important role in the coding process when the computation of physical quantities near the boundary are desired.

2.4. Higher degree polynomial shape functions of the boundary values

To assure the non-existence of boundary layer in boundary integrals, higher degree polynomial shape functions of the boundary values are employed in new formulation of the integration analytically. It can be easily observed that higher order polynomial terms can be reduced to similar terms of linear elements with the following equation [35]:

$$\begin{aligned}
\int x^{m+1}(a + bx^n)^p \mathrm{d}x = &\frac{1}{b(m+np)}[x^{m-n}(a + bx^n)^{p+1} \\
&- (m-n)a \int x^{m-n-1}(a + bx^n)^p \mathrm{d}x]
\end{aligned} \qquad (17)$$

In present case, $a = \eta_i^2$, $b = 1$, $n = 2$, $p = -1$, $x = \xi$, that is

$$\int \left(\frac{\xi^{m-1}}{\xi^2 + \eta_i^2}\right)\mathrm{d}\xi = \left(\frac{1}{m-2}\right)\xi^{m-2} - \eta_i^2 \int \left(\frac{\xi^{m-3}}{\xi^2 + \eta_i^2}\right)\mathrm{d}\xi \quad (m \geq 3) \qquad (18)$$

Thus, for any higher-degree shape function, the high degree terms can be reduced to the zeroth, first- and second-degree terms easily, which Liggett and Liu [4] had described in analytical forms. As the source point approaches to the boundary (i.e. $\eta_i \to 0$), the second term in Eq. (18) converges to zero and the first term is finite. Thus, the error in evaluation of the arc-tangent term appears only in the zeroth degree term, but not in higher-degree integration. That is, there will not be any additional value contributed to the coefficient of potential from the higher-degree terms.

3. Physical singularities in BEM

Physical singularities arise from the degenerated boundary or a change in boundary condition [36]. A typical example is illustrated in Fig. 4(a). When water flows in channel (1) with straight and smooth boundaries, the potential and derivative of potential can be obtained everywhere, without the singularity problem. However, as the boundaries degenerate, like channel (2), a multi-value problem will appear accordingly at the vertices, and the defining of the potential derivatives becomes difficult. The phenomenon originates from drastic boundary variations. To distinguish this with mathematical singularities, they are termed as 'physical singularities'. For potential

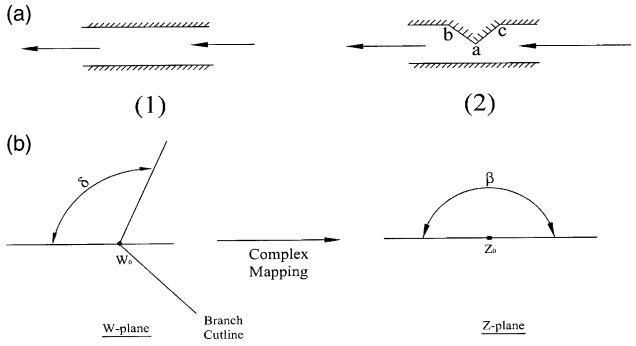

Fig. 4. (a) Illustration of physical singularities. (b) Complex mapping from W-plane to Z-plane.

problems, it is worth noting that the potential lines and streamlines passing three points a, b and c are not orthogonal, implying multi-derivative values, even though the potentials on those points are unique. Furthermore, at point a, the behavior of potential value is focusing while the potentials are diverging at points b and c. These kinds of physical singularities at b, c and a can be called as 'weak singularities' and 'strong singularities', respectively.

The singularity problem mentioned above derives from the corner containing two Dirichlet boundaries, is also called 'geometrical singularity'. However, physical singularity is not confined to the geometric singularity. When mixed boundary conditions (for example, Dirichlet condition on an element and Neumann condition on its neighboring element), are imposed on a smooth boundary, the normal gradient is still undefined at the intersection of these two elements, that is, the stream lines and the potential lines for potential flow are still not perpendicular to each other, then the physical singularity exists but there is no geometrical singularity. Under these circumstances, one has to use special techniques to resolve the normal gradient at the singular points in case using conforming elements [37].

In the past few years, the classification of mathematical singularities and physical singularities are obscure. Usually, they are treated collectively and are called singularity problems. In fact, only physical singularity (geometric singularity) exists in the BEM as the non-existence of mathematical singularities has just been proved.

Several methods have been proposed to resolve physical singularity problems [31–33]. However, a simple complex mapping technique is presented in this section.

By using complex transform from W-plane to Z-plane as shown in Fig. 4(b), the effect of physical singularities can be overcome easily [38]

$$Z - Z_0 = \frac{\delta}{\beta}(W - W_0)^{\beta/\delta} \tag{19}$$

where δ is the angle between two straight lines to be transformed on the original W-plane and β is the transformed angle on the Z-plane. W_0 and Z_0 are the branch points on the W-plane and Z-plane, respectively. The physically singular point is represented as W_0 and the angle of the degenerated boundary on W-plane is transformed into designated angles such as π or $\pi/2$ on Z-plane. The points of these two straight lines are also transformed to Z-plane. The procedures are applied repeatedly until the original domain is transformed into a hyper-rectangular area, which consists of four smooth boundaries with four right corner angles [38]. These procedures eliminate possible physical singularities and prepare a perfect domain for potential functions. The potential can be calculated in the Z-plane by using BEM, including all the boundary points. Results of potentials and its derivatives on the W-plane are obtained by inverse mapping of Eq. (19). The derivatives of the potential on Z-plane, however, should be multiplied by a Jacobian factor in the inverse transformation to the W-plane.

For comparisons, four nodal-point allocation strategies to improve accuracy in a problem with physical singularities are proposed. That is, The singular-point elements divided method (SED), overall elements divided (OED), mapping and singular-point elements divided (MSED), and mapping and overall elements divided (MOED).

The SED is a strategy of nodal points allocation by adding points that divide merely the elements next to the physically singular points in each computation. And, the iterations are repeated until the absolute error is below a threshold. Similarly, the OED is developed to divide every boundary element into one half in each run. The MSED is a method to implement the SED after the complex mapping. So does the MOED to the OED after the complex mapping.

Among the four strategies, two methods containing complex mappings can largely reduce the errors thanking to the physical singularities. However, it may result in the non-linearity when a linear boundary is transformed into the corresponding non-linear boundary by complex mapping. For general cases, the former error will be greater than the latter one. Thus, MSED and MOED are much more efficient in the treatment of singularity problems. This is to be discussed in detail in Section 4.5.

4. Benchmark problems

Seven benchmark problems are presented in this section to examine the validity of present approaches. The first four benchmark problems are selected to illustrate the non-existence of numerical boundary layer. The following three problems are used to outline the complex mapping methods in treating the physical singularities. Fortran computer programs offered by Liggett and Liu are modified to perform the computations. The results are very satisfactory when compared with the exact solutions.

4.1. Standard rectangular region

As shown in Fig. 5 [4], a problem composed of rectangular boundaries with two Dirichlet boundary

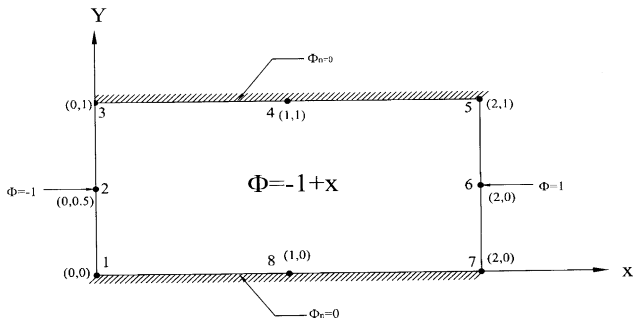

Fig. 5. Geometry and boundary conditions of the numerical example with eight-point grid system [4].

Table 1a
Numerical results for the benchmark problem of standard rectangular region using contour approach method

x	y	Computed Φ^c	Exact Φ^r	x	y	Computed Φ^c	Exact Φ^r
0.0	0.0	−1.000000000	−1	1.0	0.6	0.000000002	0
0.0	0.2	−1.000000000	−1	1.0	0.8	0.000000001	0
0.0	0.4	−1.000000000	−1	1.0	1.0	0.000000003	0
0.0	0.6	−0.999999900	−1	1.5	0.0	0.500000000	0.5
0.0	0.8	−1.000000000	−1	1.5	0.2	0.500000000	0.5
0.0	1.0	−1.000000000	−1	1.5	0.4	0.500000000	0.5
0.5	0.0	−0.500000000	−0.5	1.5	0.6	0.500000000	0.5
0.5	0.2	−0.500000000	−0.5	1.5	0.8	0.500000000	0.5
0.5	0.4	−0.500000000	−0.5	1.5	1.0	0.500000100	0.5
0.5	0.6	−0.500000000	−0.5	2.0	0.0	1.000000000	1
0.5	0.8	−0.500000000	−0.5	2.0	0.2	1.000000000	1
0.5	1.0	−0.500000000	−0.5	2.0	0.4	0.999999900	1
1.0	0.0	0.000000029	0	2.0	0.6	0.999999800	1
1.0	0.2	0.000000006	0	2.0	0.8	0.999999900	1
1.0	0.4	0.000000007	0	2.0	1.0	0.999999800	1

$E_{\text{rms}} = \sqrt{\frac{\sum_{i=1}^{n}(\Phi_i^c-\Phi_i^r)^2}{n-1}} = 6.458\times10^{-8}$.

Table 1b
Numerical results for the benchmark problem of standard rectangular region using direct approach method

x	y	Computed Φ^c	Exact Φ^r	x	y	Computed Φ^c	Exact Φ^r
0.0	0.0	−1.000000002	−1	1.0	0.6	0.000000011	0
0.0	0.2	−1.000000006	−1	1.0	0.8	0.000000014	0
0.0	0.4	−1.000000005	−1	1.0	1.0	0.000000019	0
0.0	0.6	−1.000000002	−1	1.5	0.0	0.500000008	0.5
0.0	0.8	−0.999999999	−1	1.5	0.2	0.500000008	0.5
0.0	1.0	−0.999999992	−1	1.5	0.4	0.500000010	0.5
0.5	0.0	−0.499999998	−0.5	1.5	0.6	0.500000012	0.5
0.5	0.2	−0.499999999	−0.5	1.5	0.8	0.500000015	0.5
0.5	0.4	−0.499999999	−0.5	1.5	1.0	0.500000017	0.5
0.5	0.6	−0.499999999	−0.5	2.0	0.0	1.000000003	1
0.5	0.8	−0.499999998	−0.5	2.0	0.2	0.999999999	1
0.5	1.0	−0.499999997	−0.5	2.0	0.4	1.000000000	1
1.0	0.0	0.000000011	0	2.0	0.6	1.000000009	1
1.0	0.2	0.000000009	0	2.0	0.8	1.000000024	1
1.0	0.4	0.000000009	0	2.0	1.0	1.000000055	1

$E_{\text{rms}} = \sqrt{\frac{\sum_{i=1}^{n}(\Phi_i^c-\Phi_i^r)^2}{n-1}} = 1.401\times10^{-8}$.

conditions and two Neumann boundary conditions is taken as the first benchmark study.

By applying the two methods mentioned in the previous section with four elements, the results are presented in Table 1. It can be seen that any point in the domain can be accurately computed by these two methods, even the boundary points. The error for each point is smaller than 10^{-7} and the root-mean-square error

$$E_{\text{rms}} = \sqrt{\frac{\sum_{i=1}^{n}(\Phi_i^c - \Phi_i^r)^2}{n-1}}$$

where Φ^c is the numerical solution and Φ^r the exact solution, are as small as 6.458×10^{-8} and 1.401×10^{-8} for the two present methods. The good agreements between the numerical results and the exact solutions for the boundary points in Table 1 indicates that the two methods can directly apply to the boundary points. The main point of this example is to show that there is in fact no numerical boundary layer when using analytical analysis [4].

4.2. Triangular region problem

The problem shown in Fig. 6 [28] is composed of one Dirichlet and two Neumann boundary conditions. The equal-potential lines are parallel to the hypotenuse and the exact solution is $\Phi = x - y$. Although the geometry in this

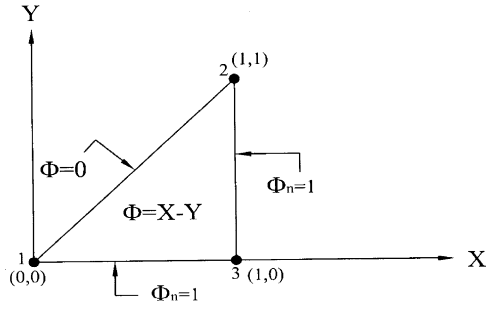

Fig. 6. Geometry and boundary conditions of the triangular region problem with three-grid system [22].

Table 2a
Numerical results for the benchmark problem of triangular region using contour approach method ($E_{rms}=5.033\times10^{-8}$)

(x,y)	Computed solution	Exact solution
(0,0)	0.000000036	0
(1,1)	0.000000061	0
(1,0)	1.000000007	1

Table 2b
Numerical results for the benchmark problem of triangular region using direct approach method ($E_{rms}=7.906\times10^{-9}$)

(x,y)	Computed solution	Exact solution
(0,0)	0.000000005	0
(1,1)	0.000000008	0
(1,0)	1.000000006	1

problem contains three corners, it is not really a so-called 'corner problem'. For there are no physical singularities in this triangular domain.

Three nodal points are used in the numerical computations. The computed potentials on the three corners agree with the exact solutions very well as shown in Table 2. And the root-mean-square errors, E_{rms}, for the contour and the direct approach methods are $E_{rms}=5.033\times10^{-8}$ and 7.906×10^{-9}, respectively.

4.3. Kisu's problem

This problem was first brought up by Kisu [7] in 1988 and was revisited by Chen [18] in 1994. It was intended to explain the boundary effect when the source point is near the boundary. A rectangular region with two Dirichlet and two Neumann boundary conditions is considered as shown in Fig. 7. The exact solution is $\Phi=0.5(x-y)$, thus $\partial\Phi/\partial x=0.5$, and $\partial\Phi/\partial y=-0.5$ everywhere.

Kisu pointed out that the nearer the source point to the boundary is, the more the results deteriorate. Also, the results of the potential gradient near the boundary become only half of the exact solutions on the boundary [7]. The problem is successfully resolved by Chen in 1994 [18] with dual boundary integral equations.

This is now known as the result of the incorrect estimation of the integral on the right hand side of Eq. (1).

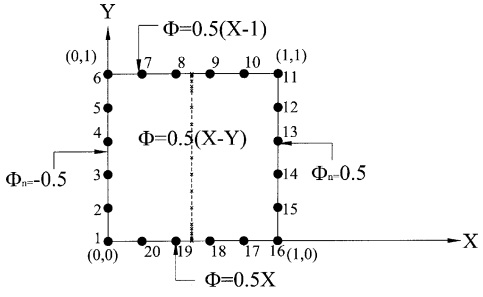

Fig. 7. Illustrative example for the boundary effect [7].

Instead of using the more complicated dual method introduced by Chen, two much simpler methods have been developed in this paper which are deemed adequate for analyzing this problem.

In present computations, only four boundary elements are adopted compared with 20 boundary elements employed by Kisu. Present results show that no matter how close the source point to the boundary, even right on the boundary, the computed potential gradient is almost the same as the analytical solution shown in Table 3. Furthermore, the root mean square errors for both present methods are as tiny as 0, 0 and 3.1×10^{-11} for potential and potential gradient values in x- and y-direction, respectively. It is such that the applicability of the present two methods in calculation of gradients is satisfactory.

4.4. Non-linear boundary's problem

This benchmark problem is selected to illustrate the application of present results on the curved boundary problem. It is a potential flow problem within an elliptical domain (Fig. 8): $x_1=2\cos\theta$ and $x_2=\sin\theta$ studied by Hang and Norio [39]. The Dirichlet boundary conditions can be obtained from the definition of potential

$$\phi=\frac{1}{2}[(x_1+1)^2+(x_2-3)^2] \tag{20}$$

Comparisons are made between present results and the results by Hang and Norio [39]. In their paper, Hang and Norio applied the modified Gauss–Tschebyscheff quadrature formula with the aid of the approximate distance function in the computations. By using 64 linear elements with 64 unknowns in our computations, the $E_{rms}=0.000076$ show that the present result is better than that by Hang ($E_{rms}=0.000173$) who used 16 cubic Hermite spline elements which consist of 64 unknowns also (Table 4).

4.5. Cut-off problem

The sheetpile cut-off wall is built commonly on the underside of a dam to prevent the seepage force. The tip of the cut-off wall is a typical example for the physical singularity. In order to make comparisons with the results by Liggett and Liu [4] and Detournay [30], a half-domain of the cut-off problem is computed first (Fig. 9). The advantage of symmetry in this problem has been taken to simplify the numerical efforts.

With complex mapping, the physical domain is transformed into a hyper-rectangular area which has four right-angle corners. Thus, the physical singularities are eliminated (Fig. 10). Under the complex non-linear mapping of Eq. (19), a straight line may be transformed into a curved one. For example, the circled point 5 standing for the strong singularity at the tip of cut-off wall on physical domain is no longer a physically singular point on the mapped domain.

Table 3a
Numerical results for Kisu's problem (1988) using contour approach method

x	y	Computed Φ	Computed $\partial\Phi/\partial x$	Computed $\partial\Phi/\partial y$
0.5	1.000000000	−0.250000000	0.500000000	−0.499999999
0.5	0.999999000	−0.249999500	0.500000000	−0.500000000
0.5	0.999990000	−0.249995000	0.500000000	−0.500000000
0.5	0.999900000	−0.249950000	0.500000000	−0.500000000
0.5	0.999000000	−0.249500000	0.500000000	−0.500000000
0.5	0.990000000	−0.245000000	0.500000000	−0.500000000
0.5	0.900000000	−0.200000000	0.500000000	−0.500000000
0.5	0.800000000	−0.150000000	0.500000000	−0.500000000
0.5	0.700000000	−0.100000000	0.500000000	−0.500000000
0.5	0.600000000	−0.050000000	0.500000000	−0.500000000
0.5	0.500000000	0.000000000	0.500000000	−0.500000000
0.5	0.400000000	0.050000000	0.500000000	−0.500000001
0.5	0.300000000	0.100000000	0.500000000	−0.500000000
0.5	0.200000000	0.150000000	0.500000000	−0.500000000
0.5	0.100000000	0.200000000	0.500000000	−0.500000000
0.5	0.010000000	0.245000000	0.500000000	−0.500000000
0.5	0.001000000	0.249500000	0.500000000	−0.500000000
0.5	0.000100000	0.249950000	0.500000000	−0.500000000
0.5	0.000010000	0.249995000	0.500000000	−0.500000000
0.5	0.000001000	0.249999500	0.500000000	−0.500000000
0.5	0.000000000	0.250000000	0.500000000	−0.500000000
E_{rms}		0	0	3.1×10^{-11}

In this case, 13 elements including 13 unknowns are taken to generate the results. To test convergence, six methods are compared, namely, the singular-point elements divided method (SED), the overall elements divided (OED), the mapping and singular-point elements divided (MSED), the mapping and overall elements divided (MOED), the singular element method by Liggett and Liu [4], and the Cauchy integral element method by Detournay [30] Physical quantities of seven points along the cut-off wall as shown in Fig. 9 are calculated. The results in Fig. 11 show that the SED is apparently superior to the OED as any one of the seven points possesses less absolute error. The inference can thus be drawn: SED is more efficient in treating a drastic variation of the potentials in the vicinity of the physically singular points.

On the other hand, as indicated by Fig. 11, both results of the MSED and the MOED present good agreement with analytical solutions, numerical results by Liggett

Table 3b
Numerical results for Kisu's problem (1988) using direct approach method

x	y	Computed Φ	Computed $\partial\Phi/\partial x$	Computed $\partial\Phi/\partial y$
0.5	1.000000000	−0.250000000	0.500000000	−0.499999999
0.5	0.999999000	−0.249999500	0.500000000	−0.500000000
0.5	0.999990000	−0.249995000	0.500000000	−0.500000000
0.5	0.999900000	−0.249950000	0.500000000	−0.500000000
0.5	0.999000000	−0.249500000	0.500000000	−0.500000000
0.5	0.990000000	−0.245000000	0.500000000	−0.500000000
0.5	0.900000000	−0.200000000	0.500000000	−0.500000000
0.5	0.800000000	−0.150000000	0.500000000	−0.500000000
0.5	0.700000000	−0.100000000	0.500000000	−0.500000000
0.5	0.600000000	−0.050000000	0.500000000	−0.500000000
0.5	0.500000000	0.000000000	0.500000000	−0.500000000
0.5	0.400000000	0.050000000	0.500000000	−0.500000001
0.5	0.300000000	0.100000000	0.500000000	−0.500000000
0.5	0.200000000	0.150000000	0.500000000	−0.500000000
0.5	0.100000000	0.200000000	0.500000000	−0.500000000
0.5	0.010000000	0.245000000	0.500000000	−0.500000000
0.5	0.001000000	0.249500000	0.500000000	−0.500000000
0.5	0.000100000	0.249950000	0.500000000	−0.500000000
0.5	0.000010000	0.249995000	0.500000000	−0.500000000
0.5	0.000001000	0.249999500	0.500000000	−0.500000000
0.5	0.000000000	0.250000000	0.500000000	−0.500000000
E_{rms}		0	0	3.1×10^{-11}

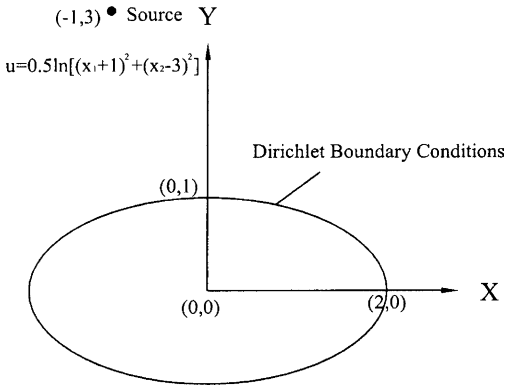

Fig. 8. Illustrative example of elliptical domain for non-linear boundary case [39].

and Liu [4], and results by Detournay [30]. The two have shown that the mapping method performs faster convergence than either by S.E.D or by the OED alone. Moreover, compared with the other points, the result of the tip of the cut-off, computed by the complex mapping methods, is especially accurate as shown in Fig. 11. It reveals the capability of complex mapping method in capturing the solutions of physically strong singular points.

Interestingly, it can also be observed from Fig. 11 that after complex mapping, the MOED is a little more accurate than the MSED, which is quite the opposite of the situation before mapping. It is possibly due to the more appropriate lineralization of the boundary elements in MOED than in MSED.

Table 4
Comparisons between present results and results by Hang and Norio [39] for a two-dimensional potential problem in an elliptic domain

Position of source point	Present results; Hang and Norio [39]; exact solutions	Relative errors	
		Present	Hang, etc.
$x_1^p = 1.9800$	1.441847	0.000004	0.000058
$x_2^p = 0.0000$	1.441768		
$d_0 = 0.0200$	1.441853		
$x_1^p = 1.0663$	1.472718	0.000052	0.000007
$x_2^p = -0.8401$	1.472651		
$d_0 = 0.005937$	1.472640		
$x_1^p = -1.5523$	0.890953	0.000056	0.000263
$x_2^p = 0.6258$	0.890770		
$d_0 = 0.004385$	0.891003		
$x_1^p = -1.9578$	1.205839	0.000055	0.000128
$x_2^p = -0.1995$	1.206033		
$d_0 = 0.001145$	1.205906		
$x_1^p = -1.5561$	0.890641	0.000099	0.000266
$x_2^p = 0.6274$	0.890503		
$d_0 = 0.00101$	0.890740		
$x_1^p = -1.9587$	1.205941	0.000078	0.000124
$x_2^p = -0.1996$	1.206143		
$d_0 = 0.0002$	1.206019		
E_{rms}		0.000076	0.000173

p, Base point; d_0, distance to the boundary.

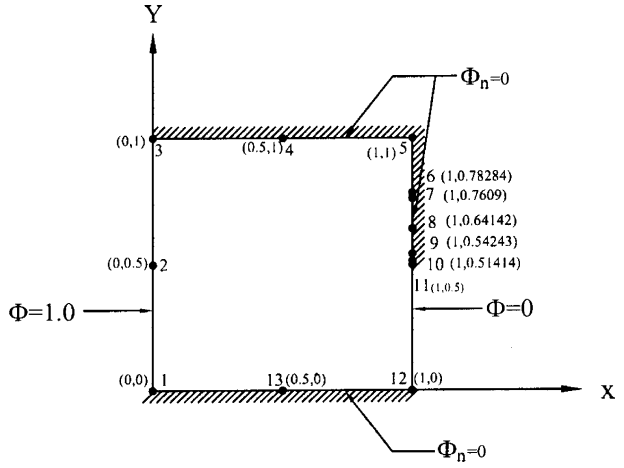

Fig. 9. Geometry and boundary conditions of the sheetpile cut-off wall problem with thirteen-point grid system [4].

The conclusion can thus be reached that the MOED is the most suitable method to solve singular problems. Therefore, the subsequent benchmark problems having physical singularities will be solved only by the MOED method, for brevity.

Because of the double elements occupying the same place along the cut-off, the singular point at the tip of cut-off wall is more difficult to be dealt with numerically when the whole-domain is taken into accounts (Fig. 12). To test applicability of present method, a whole-domain is also re-examined numerically for comparisons. There are fourteen nodal points that are used, including two elements along the cut-off wall. The validity of the methods is demonstrated again as the absolute errors are all within 10^{-2} and the improvement of the error is apparent for that the E_{rms} is reduced from 0.0025 to

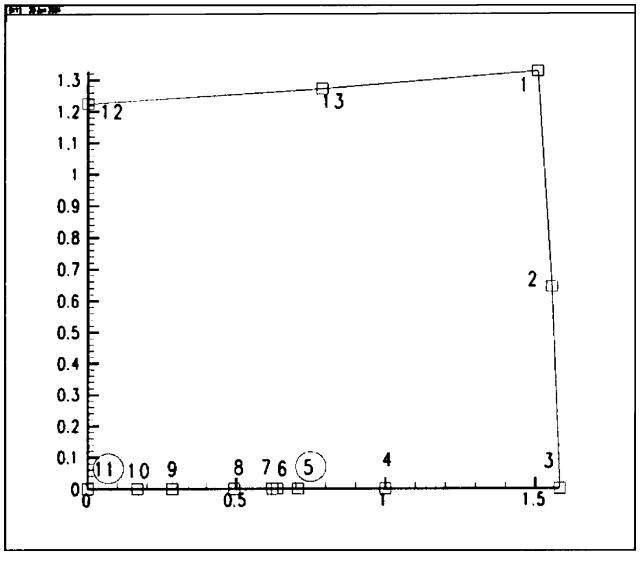

Fig. 10. Half cut-off geometry on the mapped domain.

0.0018 when compared with the result by Liggett and Liu [4]. It should be noticed that the present methods are still the traditional BEM methods with just a correct integration conception. The memory used in the computation is thus the same as the traditional one. But compared with the more complicated and time-consuming CVBEM by Detournay who used power series to simulate the complex density distribution in a Cauchy integral over the boundary element, the error is still larger as shown in Table 5.

It can be seen that the computations with the whole-domain are more accurate than that with the half one.

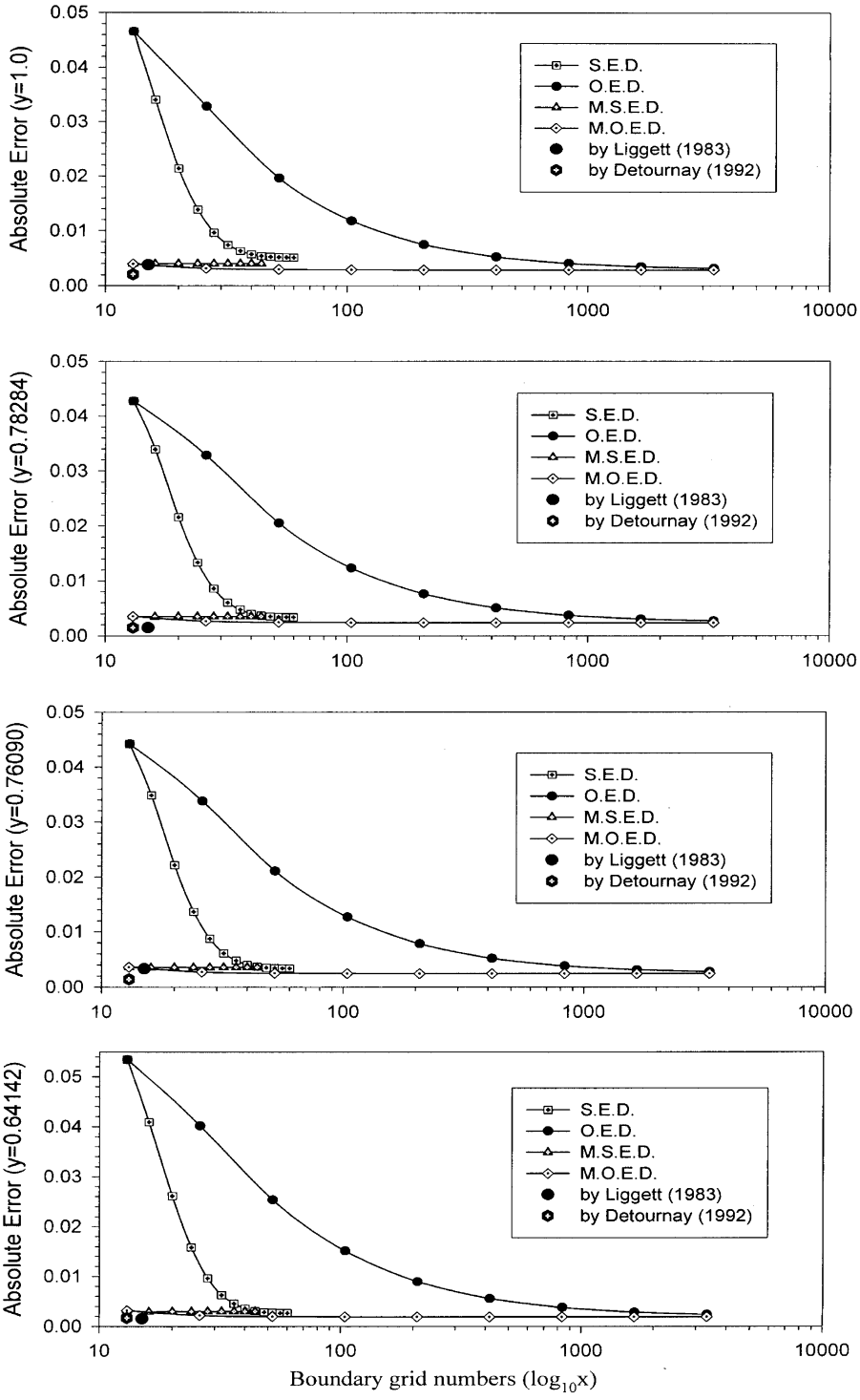

Fig. 11. Comparisons of present numerical results with other solutions.

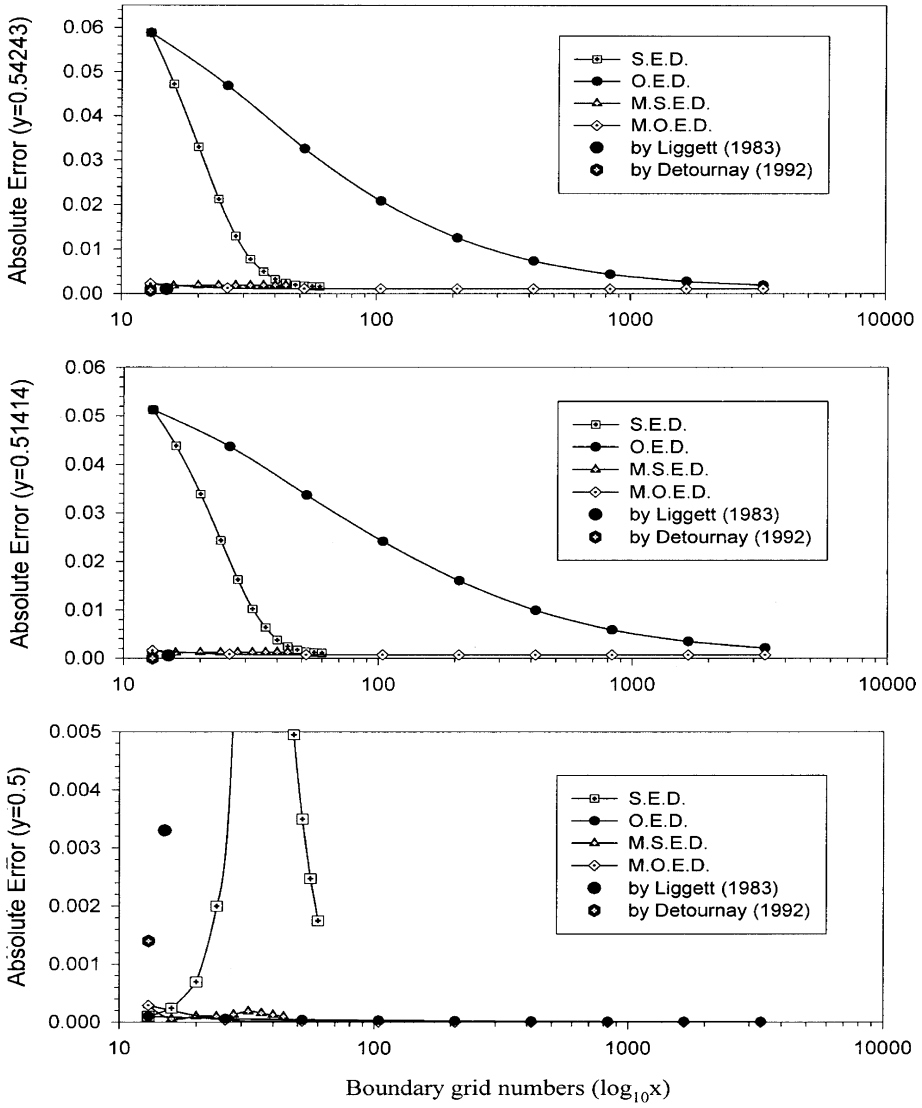

Fig. 11 (*continued*)

That may be explained by error deduction which occurs in computations with symmetrical geometries and boundary conditions.

4.6. Wedge problem

Similar to the cut-off problem, the wedge problem [4,30] is calculated and discussed with both half- and whole-domains as sketched in Fig. 13. The problem is in fact the well-known corner problem because it includes three singular corners in the whole-domain and two in the half-domain. It is noticed that, for the latter, there exist only one strong and one weak physical singularities. But for the former, there are one strong and two weak singularities instead.

Six and eight elements are adopted in the computation in half and whole-domains of wedge, respectively. The numerical results are presented in Tables 6(a) and 6(b). No solutions are calculated at the point of strong singularity by Detournay [30]. Both present results show good agreement with the exact solutions.

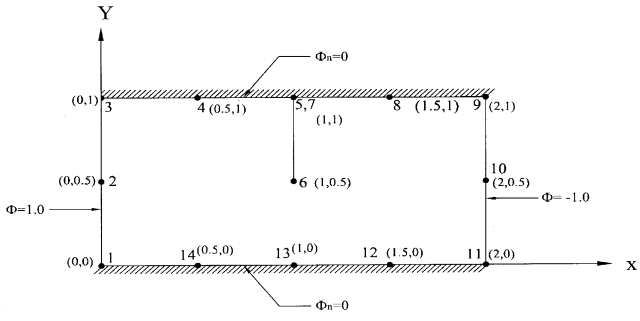

Fig. 12. Geometry and boundary conditions of the sheetpile cut-off problem with 24-point grid system [4].

Table 5
Numerical results of Φ for the whole cut-off wall problem using MOED method

y	0.5	0.51414	0.54243	0.64142	0.76090	0.78284	1.0	E_{rms}
Exact solution	0.0000	0.1096	0.1869	0.3225	0.4057	0.4159	0.4614	
Liggett and Liu	–	0.1091	0.1859	0.3210	0.4090	0.4144	0.4576	0.0025
Detournay	0.0011	0.1096	0.1862	0.3208	0.4043	0.4144	0.4593	0.0015
Present results	−0.0026	0.1075	0.1852	0.3215	0.4056	0.4161	0.4633	0.0018

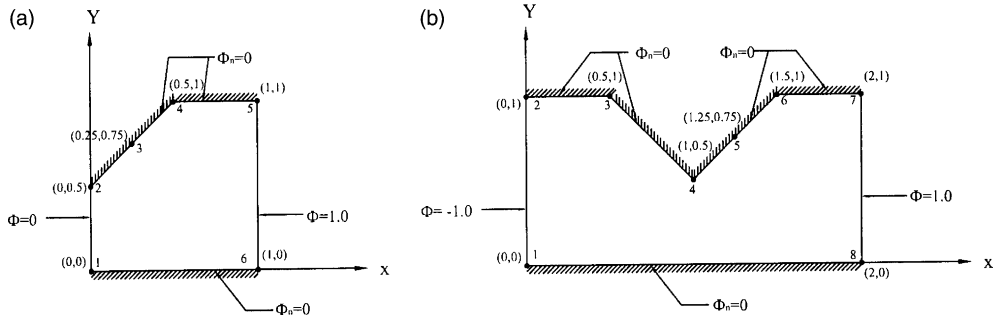

Fig. 13. (a) Geometry and boundary conditions of the right-angled wedge problem with six-point grid system; only half of the domain is considered [30]. (b) Geometry and boundary conditions of the right-angled wedge problem with eight-point grid system [30].

4.7. Motz problem

The geometry and boundary conditions of the Motz benchmark problem is shown in Fig. 14 [30,40]. Twelve elements having 12 unknowns are employed to obtain the solution. In Table 5, the present results are compared with numerical results by Detournay [30] and analytical solutions by Whiteman and Papamichael [40]. For each computed point, the error is within the order of 10^{-3} (Table 7).

To sum up, two methods developed in this paper perform very well in the calculation of the 2D potential flow problems. For references purposes, the detailed computational data are listed: all the calculations are carried out in double precision and the CPU time for the computer with T2350 Dual Processors, 256 MB RAM, and NT system ranges from $O(10^{-3})$ to 216 s for 13 elements and 1664 elements in the SED or OED methods in the half cut-off wall problem. For the other problems, the CPU time is shorter than $O(10^{-1})$ s.

Table 6a
Numerical results of Φ for the right-half wedge problem using MOED method

x	y	Exact solution; numerical, Detournay [30]; present numerical results
0	0.5	0
		–
		0.000000017
0.25	0.75	0.521
		0.522
		0.520
0.5	1.0	0.729
		0.730
		0.733

E_{rms} (Detournay) = 0.0014; E_{rms} (present) = 0.0029.

Table 6b
Numerical results of Φ for the whole wedge problem using MOED method

x	y	Exact solution; numerical solution, Detournay [30]; present numerical results
1	0.5	0
		–
		−0.000000034
1.25	0.75	0.521
		0.522
		0.519
1.5	1.0	0.729
		0.730
		0.730

E_{rms} (Detournay) = 0.0014; E_{rms} (present) = 0.0016.

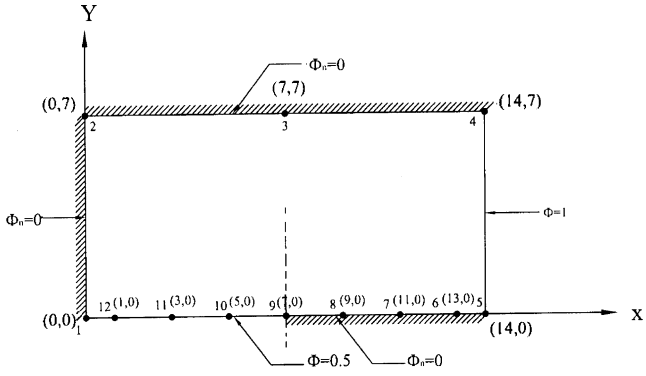

Fig. 14. Geometry and boundary conditions of the Motz problem with 12-point grid system [30].

Table 7
Numerical results for the Motz problem using MOED method

y	x						
	−6	−4	−2	0	2	4	6
6	0.5913	0.6089	0.6455	0.7021	0.7763	0.8620	0.9535
	0.5915	0.6091	0.6459	0.7022	0.7760	0.8620	0.9535
	0.5917	0.6097	0.6467	0.7033	0.7770	0.8624	0.9537
4	0.5741	0.5898	0.6248	0.6839	0.7648	0.8567	0.9520
	0.5743	0.5900	0.6249	0.6840	0.7648	0.8567	0.9520
	0.5742	0.5902	0.6254	0.6847	0.7655	0.8571	0.9522
2	0.5418	0.5520	0.5786	0.6416	0.7438	0.8486	0.9500
	0.5420	0.5522	0.5787	0.6416	0.7439	0.8486	0.9500
	0.5419	0.5521	0.5788	0.6421	0.7446	0.8490	0.9497
0	0.5000	0.5000	0.5000	0.5000	0.7285	0.8444	0.9489
	0.5000	0.5004	0.5001	0.4991	0.7290	0.8441	0.9489
	0.5010	0.5000	0.4937	0.4985	0.7299	0.8444	0.9489

Top: exact solutions; middle: Detournay [30]; bottom: present results. E_{rms} (Detournay) = 0.0003; E_{rms} (present) = 0.0014.

5. Conclusions

Singularity problems are important in many fields of applied mechanics. In this paper, the singularity problems are classified to be mathematical singularity and physical singularity. Two approaches, the contour approach and the direct approach, are developed step-by-step to prove that the mathematical singularity can be shown to vanish in the boundary element method. Thus, unlike what indicated by Liggett [4], the so-called numerical boundary layer is in fact does not exist under the analytical manipulation. Difficulties of the physical singularities including strong and weak singularities can be overcome by simple complex mapping. Numerical results of seven benchmark problems are calculated and compared with other available results to demonstrate that the potential very near the boundary (within 10^{-9} unit length) can be exactly estimated and the complex mapping method is effective mean in solving the physical singularities problems.

Acknowledgements

The authors would like to thank for financial supports from National Science Council, Taiwan under contracts Nos. NSC-87-2611-P-002-060, NSC-88-2625-Z-002-019, and NSC-89-2625-Z-002-014.

References

[1] Sladek V, Sladek J. Singular integrals in boundary element methods. UK: Computational Mechanics Publications; 1998.
[2] Guiggiani M. The evaluation of Cauchy principal value integrals in the boundary element method—a review. Math Comput Modell 1991; 15:175.
[3] Guiggiani M, Krishnasamy G, Rudolphi TJ, Rizzo FJ. A general algorithm for the numerical solution of hypersingular boundary integral equations. Trans ASME 1992;59:604.
[4] Liggett JA, Liu PL-F. The boundary integral equation method for porous media flow. UK: Allen & Unwin Ltd; 1983.
[5] Hang M, Norio K. Domain supplemental approach to avoid boundary layer effect of BEM in elasticity. Eng Anal Bound Elem. 1999;23:281.
[6] Chen HB, Lu P, Huang MG, Williams FW. An effective method for finding values on and near boundaries in the elastic BEM. Comput Struct 1998;69:421.
[7] Kisu H, Kawahara T. Boundary element analysis system based on a formulation with relative quantity. Proceedings of BEM10 conference. Southampton: Computational Mechanics Publications; 1988.
[8] Johnston PR, Elliott D. Error estimation of quadrature rules for evaluating singular integrals in boundary element problems. Int J Numer Meth Eng 2000;48:949.
[9] Nagarajan A, Mukherjee S. A mapping method for numerical evaluation of two-dimensional integrals with 1/r singularity. Comput Mech 1993;12:19.
[10] Charles TC. On bicubic transformation for the numerical evaluation of Cauchy principal value integrals. Commun Numer Meth Eng 1993; 9:307.
[11] Krishna MS, Tanaka M. On non-linear transformations for accurate numerical evaluation of weakly singular boundary integrals. Int J Numer Meth Eng 2001;50:2007.
[12] Lutz ED, Gray LJ. Analytic evaluation of singular boundary integrals without CPV. Commun Numer Meth Eng 1993;9:909.
[13] Tanaka M, Sladek V, Sladek J. Regularization techniques applied to boundary methods. Appl Mech Rev 1994;47(10):457.
[14] Gray LJ, Lutz E. On the treatment of corners in the boundary element method. J Comput Appl Math 1990;32:369.
[15] Heyliger PR, Rudolphi TJ. Evaluation of field singularities by an iterative boundary-element method. Commun Numer Meth Eng 1993; 9:337.
[16] Gupta OP, Babu SS. Error analysis in applying a boundary element method for three-dimensional steady state potential problems. Comput Struct 1996;58:289.
[17] Liang MT, Chen JT, Yang SS. Error estimation for boundary element method. Eng Anal Bound Elem 1999;23:257.
[18] Chen JT, Hong H-K. Dual boundary integral equations at a corner using contour approach around singularity. Adv Eng Softw 1994;21: 169.
[19] Gray LJ, Mamme LL. Hypersingular integrals at a corner. Eng Anal Bound Elem 1993;11:327.
[20] Chen JT. On a dual representation model and its applications to computational mechanics. PhD Thesis, Taiwan University; 1994.

[21] Ingraffea AR, Blandford G, Liggett JA. Automatic modeling of mixed-mode fatigue and quasi-static crack propagation using the boundary element method. Proc 14th Natl Symp Fract Mech 1983;971:1407.
[22] Hong H-K, Chen JT. Derivation of integral equations on elasticity. ASCE, J Eng Mech 1988;114(6):1028.
[23] Chen JT, Hong HK. On the dual integral representation of boundary value problem in Laplace equation. BE Abstracts 1993;4(3):114.
[24] Poterla A, Aliabadi MH, Rooke DP. The dual boundary element method: effective implementation for crack problems. Int J Numer Meth Eng 1992;33:1269.
[25] Crouch SL. Solution of plane elasticity problems by DD method. Int J Numer Meth Eng 1976;10:301.
[26] Gray LJ, Maroudas D, Enmark MN, D'Azevedo EF. Approximation Green's functions in boundary integral analysis. Eng Anal Bound Elem 1999;23:267.
[27] Chen JT. Singular BIE/BEM. Proceedings of BEM Conference, Section D. Taiwan: NCHC Publications; 1998.
[28] Chen JT, Hong H-K. Review of dual boundary element methods with emphasis on hypersingular integrals and divergent series. Appl Mech Rev, ASME 1999;52(1):17.
[29] Detournay C. On a Cauchy integral element method for potential flow with corner singularities. In: Computational engineering with boundary elements. Southampton; Boston: Computational Mechanics Publications; 1990 p. 119.
[30] Detournay C. A Cauchy integral element method for boundary singularities. In: Boundary element technology VII. Southampton; UK: Boston, Mass: Computational Mechanics Publications; 1992 p. 801.
[31] Papamichael N, Kokkinos CA. Two numerical methods for the conformal mapping of simply-connected domains. Comput Meth Appl Mech Eng 1981;28:285.
[32] Papamichael N, Kokkinos CA. Numerical conformal mapping of exterior domains. Comput Meth Appl Mech Eng 1982;31:189.
[33] Papamichael N, Warby MK. The treatment of corner and pole-type singularities in numerical conformal mapping techniques. J Comput Appl Math 1986;14:163.
[34] Lutz ED. Singular and nearly singular integrals. PhD Thesis, Cornell University; 1991.
[35] Peirce BO, Ronald MF. A short table of integrals. Boston: Ginn & Co.; 1956.
[36] Lefeber D. Solving problems with singularities using boundary elements. UK and Boston, MA: Computational Mechanics Publications; 1989.
[37] Karur SR, Ramachandran PA. Orthogonal collocation in the nonconforming boundary element method. J Comput Phys 1995; 121:373.
[38] Tsay TK, Hsu FS. Numerical grid generation of an irregular region. Int J Numer Meth Eng 1997;40:343.
[39] Hang M, Norio K. A general algorithm for accurate computation of field variables and its derivatives near the boundary in BEM. Eng Anal Bound Elem 2001;25(10):833.
[40] Whiteman J, Papamichael N. Treatment of harmonic mixed boundary problems by conformal transformation methods. Appl Math Phys 1972;23:655.